Interfiber Stresses in Filamentary Composites

LONGIN B. GRESZCZUK*
McDonnell Douglas Astronautics Company, Huntington Beach, Calif.

Theoretical and experimental results for the magnitude and distribution of interfiber stresses in a transversely loaded composite consisting of an elastic matrix reinforced with elastic fibers are presented. Interfiber stress distribution is also given for an inplane shear load condition. The mathematical model consists of uniformly spaced circular fibers in a square array. An approximate solution is obtained for the interfiber stresses. Theoretical results are compared with results of a photoelasticity investigation, Fil'shtinskii's rigorous elasticity solution for a plate containing rigid circular inclusions, and with results of a rigorous elasticity solution for a three-dimensional problem. The present approximate solution provides good agreement with the experimental results and with the theoretical results obtained by other authors. The method of solution presented can be used for predicting interfiber stresses in composites with various shape fibers arranged in arbitrary arrays, as well as for investigating interfiber thermal stresses, elasto-plastic deformations, and residual stresses.

Nomenclature

A_n, A_n', B_n (n = 11, 12, 13)	=	constants defined by Eqs. (23), (A23), and (A31).
E	=	Young's modulus, psi
G	=	shear modulus, psi
$E_L, E_T, G_{LT}, \nu_{LT}, \nu_{TL}$	=	principal elastic constants of unidirectional composite
$E_x, E_y, G_{xy}, \nu_{xy}, \nu_{yx}$	=	elastic constants for an element dz
k	=	fiber volume fraction of composite [$k = \pi/4(R/l)^2$]
$2l$	=	distance from center to center of fibers, in.
R	=	fiber radius, in.
ϵ	=	direct strain, in./in.
ϵ_L, ϵ_T	=	principal strains in a unidirectional composite
ϵ_x, ϵ_y	=	strains in an element dz
ν	=	Poisson's ratio
σ	=	direct stress, psi
$\sigma_L, \sigma_T, \tau_{LT}$	=	externally applied principal stresses acting on a unidirectional composite
$\sigma_x, \sigma_y, \sigma_{xy}$	=	stresses acting on an element dz
τ	=	shear stress, psi

Subscripts

x,y,z	=	coordinate axes (Fig. 1)
L,T,Z	=	axes denoting principal directions in unidirectional laminate
r	=	denotes resin or matrix material
f	=	denotes fiber material

Terminology

3-dimensional composite	=	elastic solid reinforced with continuous unidirectional fibers
2-dimensional composite	=	thin plate containing inclusions

Presented at the AIAA/ASME 11th Structures, Structural Dynamics and Materials Conference, Denver, Colo., April 22–24, 1970, (McDonald Douglas Paper 4771); submitted June 15, 1970; revision received January 11, 1971. This work was performed under the sponsorship of the McDonnell Douglas Astronautics Company-West under an Independent Research and Development Program. The author wishes to express his appreciation to W. C. Jenkins for performing the experimental photoelasticity studies.

* Staff Engineer, Advance Structures and Mechanical Department. Member AIAA.

I. Introduction

THE problem of internal stresses in plates containing inclusions made of dissimilar material has been investigated by a number of authors. Fil'shtinskii[1] presented a closed-form solution for the internal stresses in uniaxially and biaxially stressed plates containing a doubly-periodic set of circular holes, and for a plate containing rigid inclusions. The plane elasticity problem of a plate containing elastic inclusions was solved for transverse normal loading and for longitudinal shear loading by Adams and Doner.[2,3] The solution to the above problem has also been obtained by Pickett[4] using a different approach. The problem has also been studied by Shaffer[5] and Foye.[6] Most existing solutions[2–4,6] are computer solutions. These show large differences in results, as for example pointed out by Shaffer.[5]

Excellent surveys of literature on publications which can be of value in solving micromechanics problems in composite materials have been made by Wilson,[7] Goodier,[8] Eshelby,[9] and Sternberg.[10,11] Literature on the experimental investigation of internal stresses in composites is not so abundant. Some results have been reported by Daniel and Durelli,[12] as well as in Refs. 13 and 14.

This paper is not intended to provide more rigorous solution for the internal stresses in composites than those available in the literature. On the contrary, existing rigorous solutions, as well as experimental data, are used to show that the approximate solution presented herein, apart from being less complex than existing solutions, is sufficiently accurate for engineering applications. The level of sophistication involved is consistent with the accuracy of the initial assumptions which are made when solving the micromechanics problems in composites and applying the results to practical composites. These assumptions are:

1) both constituent materials obey Hooke's Law, 2) the filaments are circular, uniform in shape, and arranged in a prescribed array, 3) there are no voids in the composite, 4) the effect of microirregularities such as surface flaws, fiber misalignment, microcracks, broken filaments, etc., is negligible, and 5) both materials are homogeneous, isotropic, and are firmly bonded together.

These, or similar assumptions, are practically unavoidable when seeking useful solutions for micromechanics problems in composites, regardless of the method of solution that one may select. The inclusion of all the possible variables that are present in actual composites in the solution of the problem would constitute a monumental, if not impossible, task. Even if the resultant problem considering all the possible

variables, were solved, the complexity of the solution would limit its usefulness.

II. Theoretical Considerations

For a composite subjected to a remotely applied average transverse stress, σ_T, the conditions of symmetry require that lines *ab*, *bc*, *cd*, and *da* (Fig. 1) in the deformed composite remain parallel to the corresponding lines of the undeformed material. This implies that the gross strains over the length $2l$ in directions x and z remain constant.

$$\frac{1}{2l}\int_{-l}^{l} \epsilon_x(f,r)dx = \epsilon_T = \text{constant (at any } z) \tag{1}$$

$$\frac{1}{2l}\int_{-l}^{l} \epsilon_z(f,r)dz = \epsilon_Z = \text{constant (at any } x) \tag{2}$$

The internal stresses across the various sections will not, however, be constant but will vary as function of x and z coordinates as shown in Fig. 2. At any section across the element $2l$ the conditions of force equilibrium require that

$$\sigma_T = \frac{1}{2l}\int_{-l}^{l} \sigma_x dz \tag{3}$$

$$0 = \int_{-l}^{l} \sigma_z dx \tag{4}$$

where σ_x and σ_z are functions of z and x, respectively. The condition of force equilibrium and strain compatibility in the fiber direction, L-direction, requires that

$$\sigma_L = \frac{1}{4l^2}\int_{-l}^{l}\int_{-l}^{l} \sigma_y dx dz \tag{5}$$

$$\epsilon_y = \epsilon_L = \text{constant} \tag{6}$$

As discussed in the Appendix, the terms ϵ_x, ϵ_y, ϵ_z, σ_x, σ_y, and σ_z can be expressed in terms of stresses and strains in the matrix and the fibers, as well as fiber volume fraction k_z

$$k_z = [4k/\pi - (z/l)^2]^{1/2} \tag{7}$$

Following the procedure described in the Appendix the following approximate expressions are obtained for the interfiber stresses in three-dimensional composite material subjected to remotely applied stresses σ_L and σ_T

$$\sigma_{xr} = b_x\{(1 - \nu_{xy}\nu_{TL})(\sigma_T/E_T) + (\nu_{yx} - \nu_{LT})\sigma_L/E_L\} \tag{8}$$

$$\sigma_{yr} = [A_{13}/(1 - k_z)(A_{11} + A_{12})]\sigma_{xr} - [(A_{11} + \nu_f A_{12})/E_f k_z(1 - k_z)(A_{12}^2 - A_{11}^2)]\sigma_y \tag{9}$$

$$\sigma_{zr} = [A_{13}/(1 - k_z)(A_{11} + A_{12})]\sigma_{xr} + [(A_{12} + \nu_f A_{11})/E_f k_z(1 - k_z)(A_{12}^2 - A_{11}^2)]\sigma_y \tag{10}$$

where

$$\sigma_y = b_y[(1 - \nu_{xy}\nu_{LT})(\sigma_L/E_L) + (\nu_{xy} - \nu_{TL})\sigma_T/E_T] \tag{11}$$

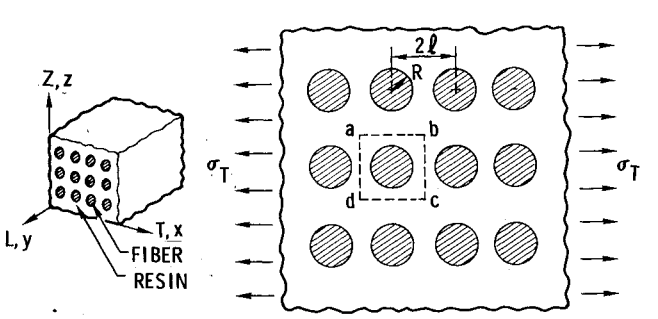

Fig. 1 Model for investigating interfiber stresses in composites.

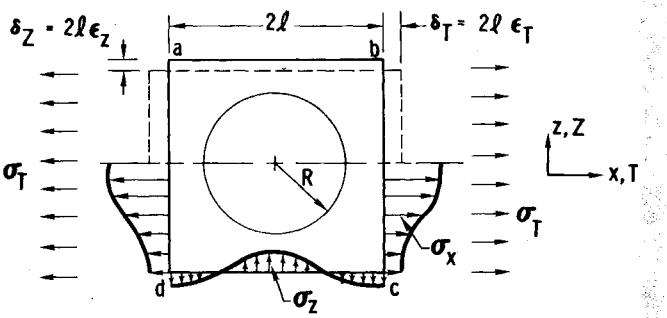

Fig. 2 Boundary stresses and deformations on a basic element.

The interfiber shear stress due to inplane shear loading can be obtained in a similar manner.[18] The final approximate expression for the shear stress is

$$\tau_{xyr} = (G_{xy}/G_{LT})\tau_{LT} \tag{12}$$

The various terms appearing in Eqs. (8–12) are defined as follows:

$$\nu_{LT} = \left(\int_{-l}^{l} \nu_{yx}b_x dz \Big/ \int_{-l}^{l} b_x dz\right) \tag{13}$$

$$\nu_{TL} = \left(\int_{-l}^{l} \nu_{xy}b_y dz \Big/ \int_{-l}^{l} b_y dz\right) \tag{14}$$

$$E_T = \frac{1}{2l}\left\{\int_{-l}^{l} b_x dz - \left[\left(\int_{-l}^{l} \nu_{xy}b_y dz\right)^2 \Big/ \int_{-l}^{l} b_y dz\right]\right\} \tag{15}$$

$$E_L = \frac{1}{2l}\left\{\int_{-l}^{l} b_y dz - \left[\left(\int_{-l}^{l} \nu_{yx}b_x dz\right)^2 \Big/ \int_{-l}^{l} b_x dz\right]\right\} \tag{16}$$

$$G_{LT} = \frac{1}{2l}\int_{-l}^{l} G_{xy} dz \tag{17}$$

where

$$b_x = E_x/(1 - \nu_{xy}\nu_{yx}), \quad b_y = E_y/(1 - \nu_{xy}\nu_{yx})$$

and in the region $0 \leq z < R$

$$\frac{1}{E_x} = \frac{1 - k_z}{E_r} + \frac{k_z}{E_f} - \frac{2A_{13}^2}{A_{11} + A_{12}} \tag{18}$$

$$\frac{1}{E_y} = \frac{A_{11} + \nu_f A_{12} + \nu_r(A_{12} + \nu_f A_{11})}{E_r E_f k_z(1 - k_z)(A_{11}^2 - A_{12}^2)} \tag{19}$$

$$\frac{\nu_{yx}}{E_{\tilde{y}}} = \frac{\nu_f}{E_f} + \frac{(1 - \nu_f)A_{13}}{k_z E_f(A_{11} + A_{12})} \tag{20}$$

$$\frac{\nu_{xy}}{E_x} = \frac{\nu_r}{E_r} - \frac{(1 - \nu_r)A_{13}}{(1 - k_z)E_r(A_{11} + A_{12})} \tag{21}$$

$$G_{xy} = G_r G_f/[G_f + k_z(G_r - G_f)] \tag{22}$$

and

$$A_{11} = 1/E_r(1 - k_z) + 1/E_f k_z \tag{23a}$$

$$A_{12} = -\nu_r/E_r(1 - k_z) - \nu_f/E_f k_z \tag{23b}$$

$$A_{13} = \nu_r/E_r - \nu_f/E_f \tag{23c}$$

$$k_z = \{(4k/\pi) - (z/l)^2\}^{1/2} \text{ or } k_z = \{(4k/\pi)[1 - (z/R)^2]\}^{1/2} \tag{24}$$

$$l = R(\pi/4k)^{1/2}$$

In the region $R < z \leq l$

$$\nu_{xy} = \nu_{yx} = \nu_r, \quad E_x = E_y = E_r, \quad G_{xy} = G_r \tag{25}$$

Equations (13–17) represent the elastic constants of a laminate in terms of the properties of the constituent materials—fibers and matrix. The integrals appearing in the

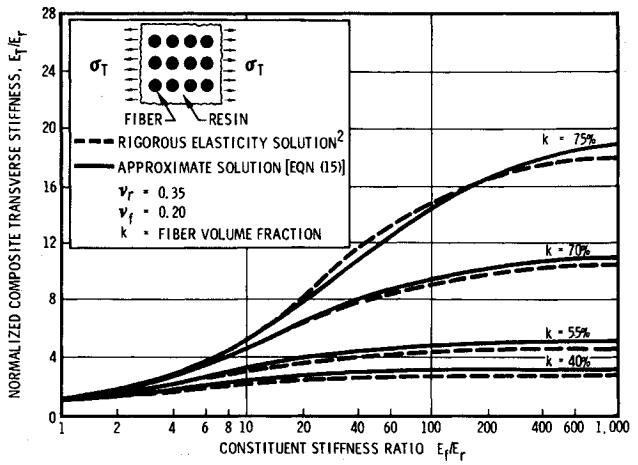

Fig. 3 Comparison of transverse composite moduli.

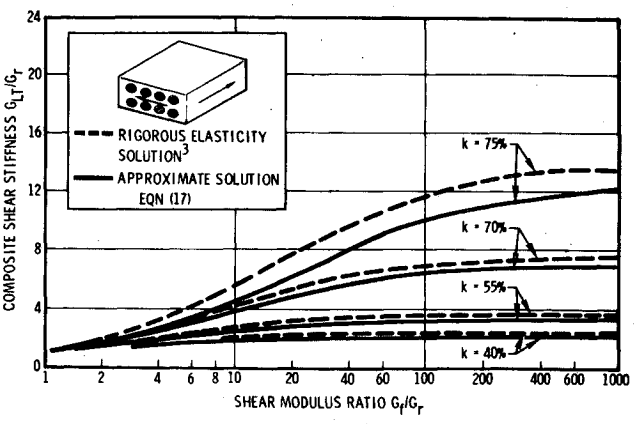

Fig. 5 Comparison of the shear moduli.

various equations can and have been evaluated numerically, using numerical integration.[15] It is noted that if the problem is simplified to a one-dimensional case, a closed-form solution can be obtained for the elastic constants and maximum stresses.[5] The three-dimensional problem does not lend itself to closed-form solution. For a two-dimensional composite simulated by a thin plate containing circular inclusions, the interfiber stresses can be derived in a similar manner. The equations for these stresses are given in the Appendix.

III. Comparison of Theoretical Results

To establish the accuracy of the approximate method of solution, the results have been compared with the results predicted by the rigorous elasticity solutions obtained by Fil'shtinskii[1] and Adams and Doner.[2,3] Figures 3 and 4 show the comparison of transverse modulus while a comparison of shear modulus is shown in Fig. 5. The comparison of the interfiber stresses in a composite subjected to transverse loading is shown in Figs. 6 and 7.

Figure 6 shows that for $(R/l) > 0.6$ ($k \gtrsim 30\%$) the maximum interfiber transverse stress remains nearly constant across the width of the matrix where the inclusions are closest together; it is slightly higher at midpoint between the fibers than it is at the fiber-matrix interface. Experimental results given in the Appendix (Fig. 13) confirm this fact.

Interfiber stresses in a solid reinforced with continuous fibers obtained herein are compared with the results of Adams and Doner[2] in Fig. 7. It is noted that Ref. 2 gives the stresses at the interface while the results obtained here are for the maximum stresses (midway between the fibers). Therefore, Fig. 7 serves only as a rough indication of the accuracy of the approximate solution.

Figure 8 shows the interfiber stresses in two- and three-dimensional composite materials containing rigid inclusions or rigid fibers. The difference in the magnitude of the maximum interfiber stress obtained from a two- and three-dimensional solution is quite small. These results also show that it is reasonable to employ two-dimensional experimental models to verify the accuracy at the three-dimensional theoretical solution for the internal stresses.

The comparison of shear stress distribution as predicted by the present [Eq. (12)] and by the rigorous elasticity solution of Adams and Doner[3] is shown in Table 1. Except for the case of $k = 0.75$, the agreement in results is quite good. The stress comparison given in Table 1 is for the same locations as shown in Fig. 6.

IV. Test-Theory Comparison

To verify the accuracy of the results, photoelasticity tests were performed on plates containing circular elastic inclusions, arranged in a square array and imbedded in an elastic matrix. The inclusions were made of 6061-T6 aluminum while the matrix material was 4290 Hysol Epoxy resin.

A two-dimensional photoelastic oblique incidence technique was used to measure the stresses across the sections of symmetry, midway between the inclusions. Prior to loading the plates in tension the fringe pattern due to residual stresses was measured. Figure 9 shows the fringe pattern due to tension and residual stresses. Superposition technique was used to obtain stresses due to externally applied loading.

The plates tested contained inclusion spacings corresponding to $k = 0.502$, 0.567, and 0.650. The comparison between the theoretical and experimental interfiber stress distribution is shown in Figs. 10 and 11. The test-theory correlation for

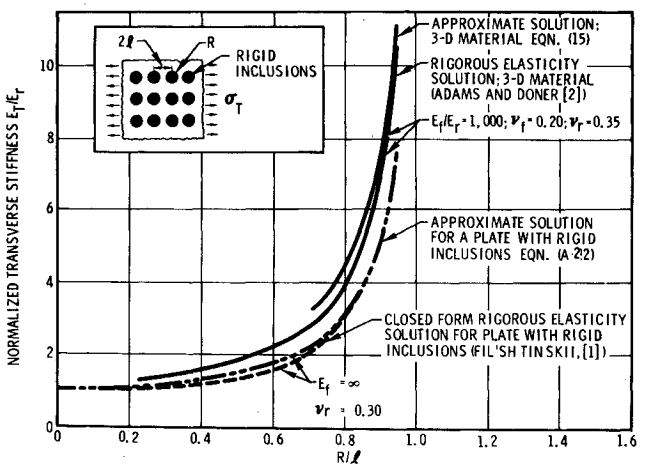

Fig. 4 Comparison of transverse moduli of a plate containing rigid inclusions.

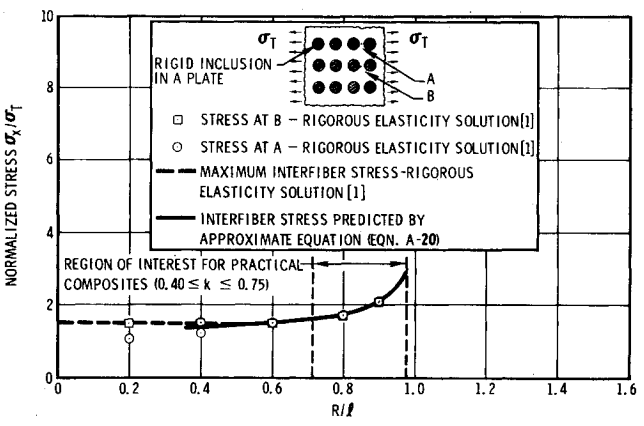

Fig. 6 Comparison of interfiber stresses.

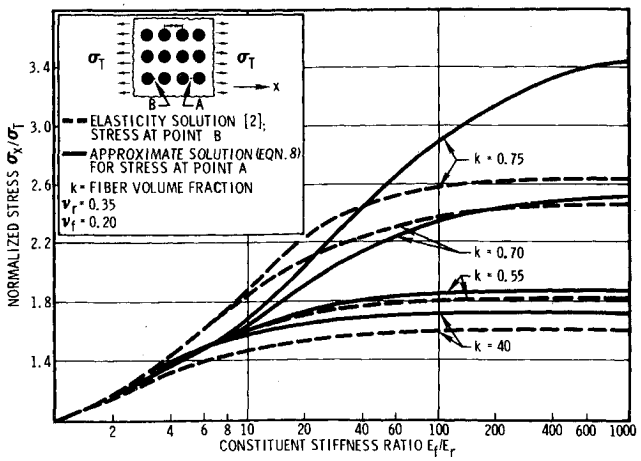

Fig. 7 Normalized maximum transverse stress in a composite containing a square array of circular elastic inclusions.

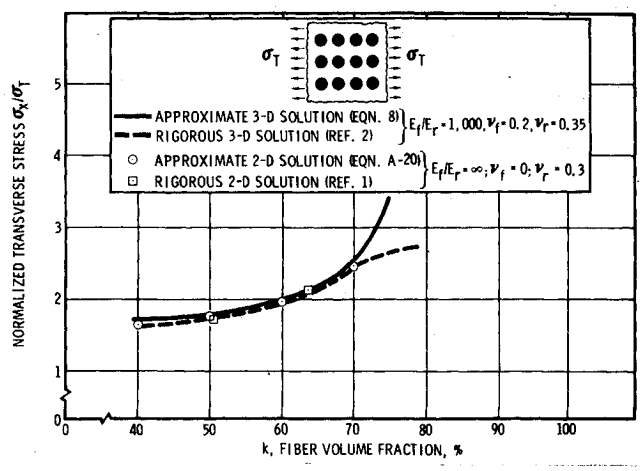

Fig. 8 Comparison of 2-D and 3-D solutions for composites containng rigid fibers/inclusions.

the maximum stress concentration between the fibers is shown in Fig. 12. The theoretical interfiber stress distribution was calculated from Eq. (8) and from equations given in the Appendix. The difference between the results obtained by the equations given in the text and those in the Appendix was negligible; 0–5% depending on the z/l. At $z/l \sim 0$, both sets of equations gave almost identical results.

The test-theory agreement shown in Figs. 10–12 is within 10%. It therefore appears, that in the range of interest ($40 \leq k \leq 75$), the approximate solution presented is sufficiently accurate for engineering applications. This applies, in particular, to actual composites where the scatter in test data and experimental errors can be in excess of 10%.

V. Conclusions

An approximate solution is presented for interfiber stresses in filamentary composites subjected to inplane shear and transverse normal loadings. The solution is shown to be sufficiently accurate for practical engineering applications (to actual composites). This is established by comparison of the results of the approximate solution with the results of a rigorous elasticity solution and with experimental results. The transverse and shear moduli predicted by the approximate theory also show good agreement with the values predicted by the rigorous theory.

Appendix: Approximate Method of Solution

To obtain an approximate solution for the interfiber stresses, one may use an approach similar to that used for determining the internal layer stresses in multilayer composites. The mathematical model is similar to those used previously for determining the approximate expressions for the elastic constants of composites.[15–18] Assuming that the basic element (Fig. 2) consists of a number of thin layers of length $2l$ and thickness dz, the stress-strain relationship for any given layer, dz, are

$$\epsilon_x = \sigma_x/E_x - \nu_{yx}(\sigma_y/E_y)$$
$$\epsilon_y = \sigma_y/E_y - \nu_{xy}(\sigma_x/E_x) \qquad \text{(A1)}$$

where E_x, E_y, ν_{xy}, and ν_{yx} are the still unknown equivalent elastic constants of an element dz, which are a function of k_z [Eq. (7)]. These can be evaluated from the following approximate equations of force equilibrium and strain compatibility which apply to any element dz

$$\sigma_{xr} = \sigma_{xf} = \sigma_x \qquad \text{(A2a)}$$
$$\sigma_{yr}(1 - k_z) + \sigma_{yf}k_z = \sigma_y \qquad \text{(A2b)}$$
$$\sigma_{zr}(1 - k_z) + \sigma_{zf}k_z = 0 \qquad \text{(A2c)}$$
$$\epsilon_{xr}(1 - k_z) + \epsilon_{xf}k_z = \epsilon_x \qquad \text{(A3a)}$$
$$\epsilon_{yr} = \epsilon_{yf} = \epsilon_y \qquad \text{(A3b)}$$
$$\epsilon_{zr} = \epsilon_{zf} = \epsilon_z \qquad \text{(A3c)}$$

The stresses appearing in Eqs. (A2) are the average stresses acting on the constituents of an element dz at any point z, and so are the strains appearing in Eqs. (A3). The variable in Eqs. (A2) and (A3) is k_z.

The use of average stresses and strains in the constituents will obviously not satisfy all the boundary conditions of the problem; e.g., all the boundary conditions at the fiber-matrix interface. Available experimental data does, however, indicate that the major assumptions, expressed by Eqs. (A2) and (A3) are reasonably accurate. The variation of σ_{xr}

Table 1 Comparison of stress concentrations due to inplane shear loading

$\tau_{xy}{}^a/\tau_{LT}$

	$k = 75\%$		$k = 70\%$		$k = 55\%$		$k = 40\%$	
G_f/G_r	Eq. (12)	Ref. 3	Eq. (12)	Ref. 3	Eq. (12)	Ref. 3	Eq. (12)	Ref. 3
1127.0	3.45	9.6	2.53	3.0	1.87	1.9	1.67	1.7
450.0	3.40	9.3	2.51	2.9	1.86	1.9	1.66	1.7
225.0	3.29	8.8	2.47	2.8	1.85	1.8	1.66	1.7
112.7	3.10	8.3	2.41	2.8	1.84	1.8	1.65	1.6
45.0	2.70	7.2	2.25	2.7	1.80	1.8	1.63	1.6
22.5	2.32	5.7	2.06	2.6	1.74	1.7	1.60	1.6
11.3	1.92	3.7	1.81	2.2	1.63	1.7	1.54	1.5
5.6	1.57	2.3	1.54	1.8	1.48	1.5	1.44	1.4

[a] τ_{xy}/τ_{LT} is the normalized stress concentration factor; τ_{LT} is the remotely applied average shear stress and τ_{xy} is the maximum interfiber shear stress.

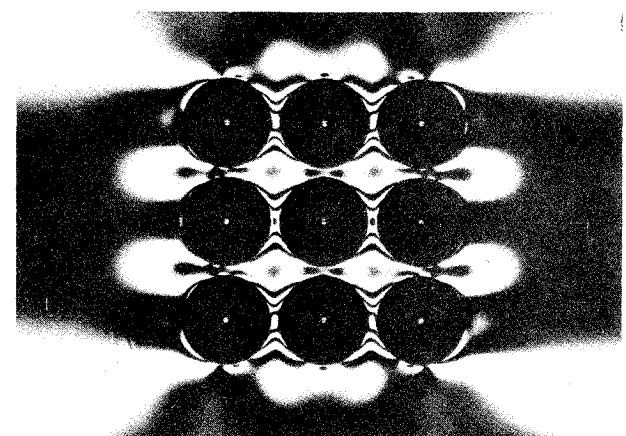

Fig. 9 Residual and uniaxial tension fringe pattern.

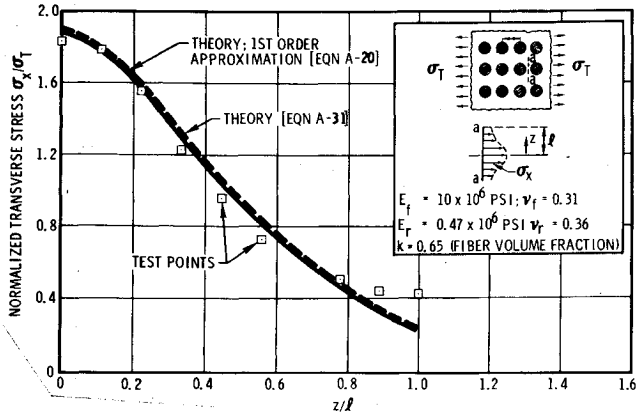

Fig. 10 Interfiber stresses; test vs theory (k = 0.65).

with x is negligible in the region of maximum stress concentration as shown in Fig. 13. Figure 13 does, therefore, partially justify the use of average stresses, σ_x, in the constituents of any element dz. This does not imply that the average stresses remain constant from element to element; on the contrary, allowance is made for the variation of σ_{xr} as a function of z (Fig. 2). On the basis of the results shown in Fig. 13, one would expect little variation in ϵ_{xr} with x; ϵ_{xr} will, however, vary with z. The validity of using average stresses in Eqs. (A2b) and (A3b) is obvious. These are the stresses and strains associated with the fiber direction, L or y. The use of average stresses and strains in Eqs. (A2c) and (A3c) is only a first approximation which can be refined as discussed later. These equations are used to account for the restraint of the matrix by the filaments in the z-direction.

To proceed with the approximate solution leading to Eqs. (13–25), the stress-strain relationships for the filament and matrix material are

$$\epsilon_{xn} = (\sigma_{xn}/E_n) - (\nu_n/E_n)(\sigma_{yn} + \sigma_{zn}) \quad \text{(A4)}$$

$$\epsilon_{yn} = (\sigma_{yn}/E_n) - (\nu_n/E_n)(\sigma_{xn} + \sigma_{zn}) \quad \text{(A5)}$$

$$\epsilon_{zn} = (\sigma_{zn}/E_n) - (\nu_n/E_n)(\sigma_{yn} + \sigma_{xn}) \quad \text{(A6)}$$

$$(n = f,r)$$

Combining Eqs. (A2–A6), three equations are obtained in σ_{yr}, σ_{zr}, and σ_{xr}. Simultaneous solution of these equations leads

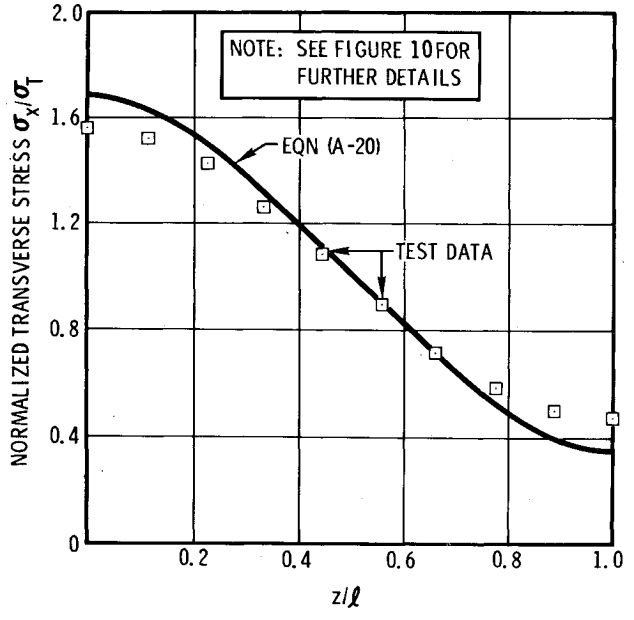

Fig. 11 Interfiber stresses; test vs theory (k = 0.502).

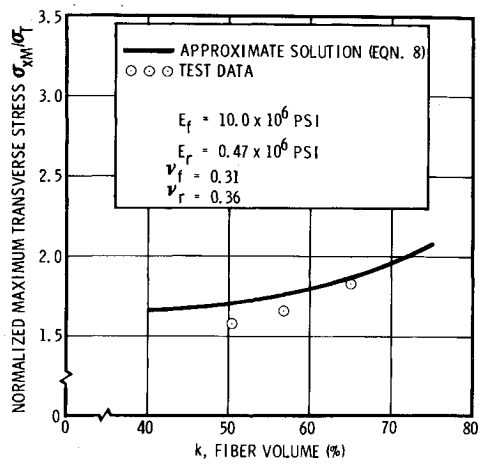

Fig. 12 Maximum interfiber stress; experiment vs theory.

to the following

$$\sigma_{zr} = [A_{13}/(1 - k_z)(A_{11} + A_{12})]\sigma_{xr} + [(A_{12} + \nu_f A_{11})/E_f k_z(1 - k_z)(A_{12}^2 - A_{11}^2)]\sigma_y \quad \text{(A7)}$$

$$\sigma_{yr} = [A_{13}/(1 - k_z)(A_{11} + A_{12})]\sigma_{xr} - [(A_{11} + \nu_f A_{12})/E_f k_z(1 - k_z)(A_{12}^2 - A_{11}^2)]\sigma_y \quad \text{(A8)}$$

$$\epsilon_x = [(1 - k_z/E_r) + (k_z/E_f) - 2A_{13}^2/(A_{11} + A_{12})]\sigma_{xr} - [(\nu_f/E_f) + (1 - \nu_f)A_{13}/k_z E_f(A_{11} + A_{12})]\sigma_y \quad \text{(A9)}$$

where A-coefficients are given by Eqs. (23). Combining Eqs. (A7, A8, A3b, and A5) yields

$$\epsilon_y = \{[A_{11} + \nu_f A_{12} + \nu_r(A_{12} + \nu_f A_{11})]/E_r E_f k_z \times (1 - k_z)(A_{11}^2 - A_{12}^2)\}\sigma_y - [\nu_r/E_r - (1 - \nu_r)A_{13}/E_r(1 - k_z)(A_{11} + A_{12})]\sigma_{xr} \quad \text{(A10)}$$

The equivalent elastic constants of an element dz can now be obtained by comparing the coefficients of Eqs. (A9), (A10), and (A1). The final results are given by Eqs. (18–21).

For an element shown in Fig. 2, the symmetry conditions require that the total strain (consisting of resin and fiber deformation) over the length $2l$ remain constant

$$\epsilon_x = \epsilon_T = \text{constant} \quad \text{(A11)}$$

$$\epsilon_y = \epsilon_L = \text{constant} \quad \text{(A12)}$$

$$\epsilon_z = \epsilon_Z = \text{constant} \quad \text{(A13)}$$

Combining Eqs. (A1, A11, and A12), multiplying both sides of

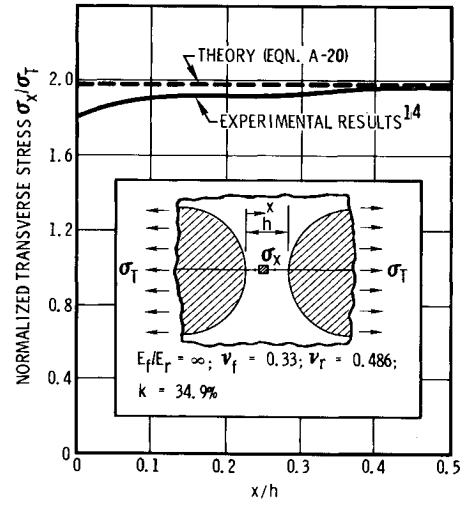

Fig. 13 Stress distribution in the matrix at the point of maximum stress concentration.

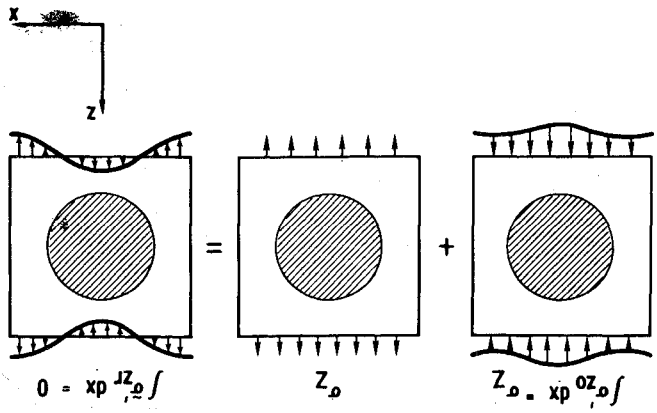

Fig. 14 Determination of stress distribution by superposition.

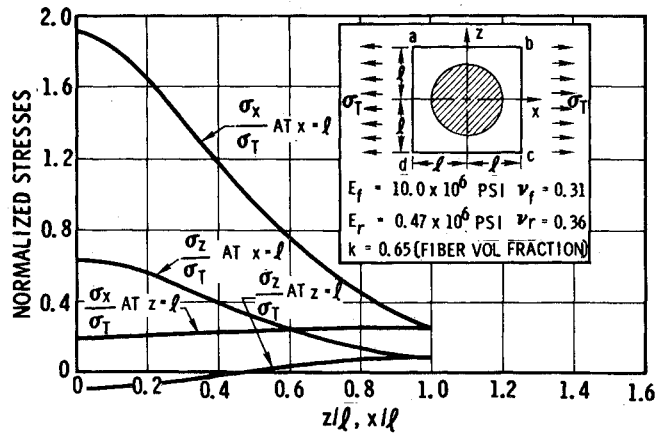

Fig. 15 Stress distribution along lines of symmetry.

the resultant equations by dz, integrating between the limits l, $-l$, and making use of Eqs. (3) and (5), one obtains

$$\sigma_L = \frac{\epsilon_L}{2l}\int_{-l}^{l} b_y dz + \frac{\epsilon_T}{2l}\int_{-l}^{l} \nu_{xy} b_y dz \qquad \text{(A14)}$$

$$\sigma_T = \frac{\epsilon_T}{2l}\int_{-l}^{l} b_x dz + \frac{\epsilon_L}{2l}\int_{-l}^{l} \nu_{yx} b_x dz \qquad \text{(A15)}$$

where b_x and b_y are defined after Eq. (17).

The conventional stress-strain relationship for a monofilament laminate can be expressed as

$$\sigma_L = (E_L/1 - \nu_{LT}\nu_{TL})\epsilon_L + (\nu_{TL}E_L/1 - \nu_{LT}\nu_{TL})\epsilon_T \qquad \text{(A16)}$$

$$\sigma_T = (E_T/1 - \nu_{LT}\nu_{TL})\epsilon_T + (\nu_{LT}E_T/1 - \nu_{LT}\nu_{TL})\epsilon_L \qquad \text{(A17)}$$

Comparison of coefficients in Eqs. (A14) and (A15) with the coefficients in Eqs. (A16) and (A17) gives the final expressions for E_L, E_T, ν_{LT}, and ν_{TL} shown by Eqs. (13–16).

To obtain interfiber stresses at section b-c (Fig. 1), as a function of the z-coordinate, Eqs. (A1) are first solved for σ_x and σ_y

$$\sigma_x = [(E_x/1 - \nu_{xy}\nu_{yx})](\epsilon_x + \nu_{yx}\epsilon_y) \qquad \text{(A18)}$$

$$\sigma_y = [(E_y/1 - \nu_{xy}\nu_{yx})](\epsilon_y + \nu_{xy}\epsilon_x) \qquad \text{(A19)}$$

Substitution of Eqs. (A11) and (A12) for ϵ_x and ϵ_y followed by a combination of the resultant equations with Eqs. (A16) and (A17) yields the equations for the stresses σ_x and σ_y in an element dz. Combining the resultant equations for σ_x and σ_y with Eqs. (A7–A9) leads to the final expression given by Eqs. (9, 10, and 11).

A similar procedure has been used to determine the internal stresses due to inplane shear loading and also the interfiber stresses in a plate containing circular inclusions. For the case of a plate containing circular elastic inclusions arranged in a square array and subjected to transverse normal loading the final results for the interfiber stresses are

$$\sigma_{xr}' = E_x'(\sigma_T/E_T') \qquad \text{(A20)}$$

$$\sigma_{zr}' = [A_{13}E_x'/A_{11}(1 - k_z)](\sigma_T/E_T') \qquad \text{(A21)}$$

where

$$E_T' = \frac{1}{2l}\int_{-l}^{l} E_x' dz \qquad \text{(A22a)}$$

$$E_x' = A_{11}/(A_{11}A_{12}' - A_{13}^2) \qquad \text{(A22b)}$$

$$\nu_{TZ} = \frac{1}{l}\int_{0}^{l} \nu_{xz}' dz \qquad \text{(A22c)}$$

$$\nu_{xz}' = -[A_{13} - \nu_r(1 - k_z)A_{11}]/E_r(1 - k_z)(A_{11}A_{12}' - A_{13}^2) \qquad \text{(A22d)}$$

where in addition to previously defined terms A_{11} and A_{13}

$$A_{12}' = k_z/E_f + (1 - k_z)/E_r \qquad \text{(A23)}$$

and the terms with primes refer to a two-dimensional composite.

The average stresses in the z-direction in any given element dz were assumed to be independent of the x-coordinate. To obtain the variation of σ_z' in the x-direction, superposition as shown in Fig. 14 can be used. The relationship between the remotely applied stress σ_Z and the stress σ_{zo}' (corresponding to the first approximation) at any point x is

$$\sigma_{zo}' = (E_z'/E_Z')\sigma_Z \qquad \text{(A24)}$$

where E_z' and E_Z' can be obtained from Eqs. (A22) by replacing subscripts x with z and T with Z. By superposition the net stress at any point x is

$$-\sigma_{zo}' + \sigma_Z = \sigma_z' \qquad \text{(A25)}$$

or, in view of Eq. (A24)

$$\sigma_z' = [1 - (E_z'/E_Z')]\sigma_Z \qquad \text{(A26)}$$

It can be readily shown that Eq. (A26) satisfies equilibrium condition expressed by Eq. (4). To satisfy the relationship

$$\epsilon_Z = -\nu_{TZ}'\epsilon_T \qquad \text{(A27)}$$

requires that the still unknown σ_Z satisfy the following

$$\sigma_Z = \nu_{TZ}'\sigma_T E_Z'/E_T' \qquad \text{(A28)}$$

Combining Eqs. (A28) with (A26) and noting that for a square fiber array $E_Z' \equiv E_T'$ yields

$$\sigma_z' = [1 - (E_z'/E_T')](\nu_{TZ}'\sigma_T) \qquad \text{(A29)}$$

which is the final expression for the distribution of stresses along lines ab and cd (Fig. 1). The stress distribution along lines ad and bc is given by Eq. (A20). The stress σ_z' will also induce stresses in the x direction. Using superposition, the final expression for the stress distribution in the x and z directions are

$$\tilde{\sigma}_{zr}' = -[(E_T' - E_z')\nu_{TZ}' + A_{13}E_x'/A_{11}(1 - k_z)]\sigma_T/E_T' \qquad \text{(A30)}$$

$$\tilde{\sigma}_{xr}' = [E_x' + [B_{13}/B_{11}(1 - k_z)](E_T' - E_z')\nu_{TZ}']\ \sigma_T/E_T' \qquad \text{(A31)}$$

where the terms B_{11}, B_{13}, and E_z' are a function of k_x, the terms A_{11}, A_{13}, and E_x' are a function of k_z and

$$k_n = [(4k/\pi) - (n/l)^2]^{1/2}$$

where $n = x$ or z. The terms B_{11}, B_{13}, and E_z' can be obtained from the expressions A_{11}, A_{13}, and E_x' [Eq. (A22)] by replacing k_z with k_x.

The approach described above can also be applied to refine the analysis for the internal stresses in three-dimensional composites. However, the difference in results calculated by the equations corresponding to the first and second approximations [Eq. (A20) vs Eq. (A31)] is small as shown in Fig. 10. The stress distribution along lines *ab* and *bc* (see Fig. 1) is shown in Fig. 15.

References

[1] Fil'shtinskii, L. A., "Stresses and Displacements in an Elastic Sheet Weakened by a Doubly-Periodic Set of Equal Circular Holes," *Prikladnaia Mathematika i Mekhanika*, Vol. 28, No. 3, 1964, pp. 430–441.

[2] Adams, D. A. and Doner, D. R., "Transverse Normal Loading on a Unidirectional Composite," *Journal of Composite Materials*, Vol. 1, No. 2, 1967, pp. 152–164.

[3] Adams, D. A. and Doner, D. R., "Longitudinal Shear Loading of a Unidirectional Composite," *Journal of Composite Materials*, Vol. 1, No. 1, 1967, pp. 4–18.

[4] Pickett, G., "Elastic Moduli of Fiber Reinforced Plastic Composites," *Fundamental Aspects of Fiber Reinforce Composites*, edited by R. T. Schwartz, Interscience, New York, 1968, pp. 13–27.

[5] Shaffer, B. W., "Elasto-Plastic Stress Distribution Within Reinforced Plastics Loaded Normal to Its Internal Filaments," *AIAA Journal*, Vol. 6, No. 12, 1968, pp. 2316–2324.

[6] Foye, R. B., "Structural Composites, Quarterly Progress Repts. 1 and 2, "USAF Contract AF 33(615)-5150, 1966, Air Force Materials Lab., Wright-Patterson Air Force Base, Ohio.

[7] Wilson, H. B., "Mathematical Studies of Composite Materials," S-42, Dec. 1963, Rohm and Haas Co., Huntsville Ala.

[8] Goodier, J. N., "A Survey of Some Recent Researches in Theory of Elasticity," *Applied Mechanics Review*, Vol. 4, 1951, pp. 330–332.

[9] Eshelby, J. D., "Elastic Inclusions and Inhomogeneities," *Progress in Solid Mechanics*, Vol. 2, North Holland Publishing, Amsterdam, 1961, pp. 89–140.

[10] Sternberg, E., "Three-Dimensional Stress Concentrations in the Theory of Elasticity," *Applied Mechanics Review*, Vol. 1, 1958, pp. 1–4.

[11] Sternberg, E., "On Some Recent Developments in the Linear Theory of Elasticity," *Structural Mechanics*, Pergamon Press, New York, 1960, pp. 48–73.

[12] Daniel, I. M. and Durelli, A. J., "Photoelastic Investigation of Residual Stresses in Glass Plastic Composites," *Proceedings of the 16th Annual Conference of the Society of Plastics Industry*, Sec. 19A, 1961.

[13] "Structural Airframe Applications of Advanced Composites; Fourth Quarterly Progress Report," AFML Contract AF33(615)-5257, June 1967, ITT Research Inst., Texaco Experiment, Inc., and General Dynamics.

[14] "Study of Mechanical Properties of Solid Rocket Grains," Rept. 0411-10F, prepared under contract AF33(600)-40314S. A. No. 1, March 1962, Aerojet General.

[15] Greszczuk, L. B., "Thermoelastic Properties of Filamentary Composites," *6th AIAA Structures and Materials Conference*, Palm Springs, Calif., 1965.

[16] Paul, B., "Prediction of Elastic Constants of Multiphase Materials," *Transactions* AIME, Vol. 218, 1960, p. 36.

[17] Ekvall, J. C., "Elastic Properties of Orthotropic Monofilament Laminates," Paper 61-AV-56, *Proceedings of ASME Aviation Conference*, Los Angeles, Calif., 1961,

[18] Greszczuk, L. B., "Elastic Constants and Analysis Methods for Filament Wound Shell Structures," Rept. SM-45849, Jan. 1964, Douglas Aircraft Co.

JULY 1971 AIAA JOURNAL VOL. 9, NO. 7

A Study of Hypersonic Corner Flow Interactions

RALPH D. WATSON* AND LEONARD M. WEINSTEIN†
NASA Langley Research Center, Hampton, Va.

Characteristics of the hypersonic flowfields over three sharp leading-edge internal corner models have been measured at Mach 20 in helium. Wedges of equal angles (0°–0°, 5°–5°, and 10°–10°) intersecting at 90° formed the models. The measurements include heat-transfer and surface pressure distributions, Pitot surveys in the base plane of the models, oil-flow photographs, and electron beam flow visualization photographs. The data indicate that the broad features of external and internal shock structure observed at supersonic Mach numbers also occur at Mach 20; however, the presence of large vortices and thick boundary layers distort the flow in the immediate vicinity of the corner. Observed peaks in surface heat transfer correlate with a strong vortex near the corner and a disturbance propagated from the inviscid flow into the boundary layer. The flowfield appears to be basically conical in nature except for large values of $\bar{\chi}$ the hypersonic viscous interaction parameter. Corner heating rates, relative to undisturbed wedge or flat-plate heating rates, increase significantly with increasing freestream Mach number.

Nomenclature‡

C = Chapman-Rubesin constant
M = Mach number
P = pressure
Pr = Prandtl number
$\dot{q}$ = heat flux
R = Reynolds number
T = temperature
x,y,z = Cartesian coordinates
$\bar{y},\bar{z}$ = orthogonal coordinates measured from the corner juncture
α = angle between wedge and freestream vector
γ = ratio of specific heats
δ = Pitot boundary-layer thickness
δ^* = displacement thickness
ϕ = wedge intersection angle, measured in y-z plane
$\bar{\chi}$ = viscous interaction parameter

Presented as Paper 70-227 at the AIAA 8th Aerospace Sciences Meeting, New York, January 19–21, 1970; submitted March 2, 1970; revision received March 15, 1971.

* Aerospace Engineer, Hypersonic Vehicles Division. Member AIAA.
† Aerospace Engineer, Hypersonic Vehicles Division.

‡ Primes denote reference temperature value.